PASJ: Publ. Astron. Soc. Japan **63**, 53–61, 2011 February 25

Internal Proper Motions of Methanol Masers at 6.7 GHz in Massive Star-Forming Region Onsala 1

Koichiro SUGIYAMA,[1] Kenta FUJISAWA,[1,2] Akihiro DOI,[3,4,2] Mareki HONMA,[5,6] Yasuko ISONO,[7,1] Hideyuki KOBAYASHI,[5,8] Nanako MOCHIZUKI,[3] Yasuhiro MURATA,[3,4] Satoko SAWADA-SATOH,[8,1] and Kiyoaki WAJIMA[1,2]

[1]*Graduate school of Science and Engineering, Yamaguchi University, 1677-1 Yoshida, Yamaguchi, Yamaguchi 753-8512*

[2]*Department of Physics, Faculty of Science, Yamaguchi University, 1677-1 Yoshida, Yamaguchi, Yamaguchi 753-8512*

[3]*The Institute of Space and Astronautical Science, Japan Aerospace Exploration Agency, 3-1-1 Yoshinodai, Chuo-ku, Sagamihara 229-8510*

[4]*Department of Space and Astronautical Science, Graduate University for Advanced Studies, 3-1-1 Yoshinodai, Chuo-ku, Sagamihara 229-8510*

[5]*VERA Project, National Astronomical Observatory of Japan, 2-21-1 Osawa, Mitaka, Tokyo 181-8588*

[6]*Department of Astronomical Science, Graduate University for Advanced Studies, 2-21-1 Osawa, Mitaka, Tokyo 181-8588*

[7]*Solar-Terrestrial Environment Laboratory, Nagoya University, Furocho, Chikusaku, Nagoya, 464-8601*

[8]*Mizusawa VLBI Observatory, 2-12 Hoshigaoka, Mizusawa, Oshu, Iwate 023-0861*

m005wa@yamaguchi-u.ac.jp

(Received 2010 May 18; accepted 2010 December 16)

Abstract

We present the internal proper motions of 6.7 GHz methanol masers in a massive star-forming region, Onsala 1 (ON 1), measured using the Japanese very long baseline interferometry network (JVN) at three epochs spanning 778 days. The methanol masers were clearly distinct from water masers. The methanol masers surrounded an ultra-compact (UC) H II region, and their distribution was similar to that of hydroxyl masers. The internal motions of the methanol masers were clearly detected; they show outward motions in roughly the north–south direction with a relative velocity of $\sim 5\,\mathrm{km\,s^{-1}}$. Their motion is similar to that of hydroxyl masers, which showed expansion at $\sim 5\,\mathrm{km\,s^{-1}}$, and these two types of masers seem to trace the expanding UC H II region. Another possibility is that the methanol masers are associated with a molecular outflow observed by $H^{13}CO^+$ and SiO lines, because the direction and velocity of the methanol masers were similar to those of the molecular lines. Regarding the relative phases of water and methanol masers in the evolutionary stage of massive young stellar objects, we found that the former was earlier than the latter in ON 1 by comparing the sites associated with the masers. The water masers were associated with dust emission at submillimeter wavelengths, whereas the methanol masers were associated with an UC H II region at centimeter wavelengths, which appears at a later evolutionary phase than the dust core.

Key words: ISM: H II regions — ISM: individual (Onsala 1) — masers: methanol

1. Introduction

Methanol masers at 6.7 GHz have been detected only in massive star-forming regions (Minier et al. 2003; Xu et al. 2008). They are thought to trace the period just before, or early in the ultra-compact (UC) H II region phase (e.g., Walsh et al. 1998). Therefore, they can be a useful tool for investigating star formation around massive young stellar objects (YSOs). It has been suggested that the 6.7 GHz methanol masers appear at an earlier evolutionary phase in massive star formation than 22.2 GHz water masers (Ellingsen et al. 2007 and references therein). Beuther et al. (2002) superposed the distributions of the 6.7 GHz methanol masers on those of the 22.2 GHz water masers, the millimeter dust continuum, the centimeter continuum, and mid-infrared sources in massive star-forming regions with absolute positional accuracies of $\sim 1''$. The results supported the suggestion that the methanol masers appear at an earlier stage than the water masers. On the other hand, Reid (2007) suggested that the water masers trace an earlier stage than the methanol masers.

Various morphologies of the 6.7 GHz methanol masers have been observed. The linear spatial structure and linear velocity gradient of the maser spot distribution have often been interpreted as being an edge-on Keplerian rotating disk (e.g., Minier et al. 2000). However, these characteristics are not observed for 60% of methanol maser sources. Phillips et al. (1998) and Walsh et al. (1998) suggested a shock-wave model with low velocities for those sources. Other evidence of association with shock regions was reported by De Buizer (2003), Dodson et al. (2004), and Surcis et al. (2009). The masers also exhibit the following morphology and kinematics: ring-like structures (Bartkiewicz et al. 2005, 2009; Sugiyama et al. 2008a; Torstensson et al. 2008, 2010), infall (Goddi et al. 2007; Vlemmings et al. 2010), and rotating toroids (Moscadelli et al. 2007).

Measuring the internal proper motions of methanol masers is essential for studying not only the associated sites, but also the evolution of massive YSOs. We have conducted very long baseline interferometry (VLBI) monitoring of 6.7 GHz methanol masers in a massive star-forming region Onsala 1 (ON 1, section 2) by using the Japanese VLBI network (JVN: Fujisawa 2008), and measured their internal proper motions.

We describe these observations and the data reduction in detail in section 3. In section 4, we present their spatial distribution and internal proper motions measured at three epochs spanning 778 days. Finally, we discuss the sites associated with the masers in ON 1 in section 5 on the basis of the superposition of other probes and measurements of the proper motions.

2. ON 1

The massive star-forming region ON 1 is located at a distance of $2.57^{+0.34}_{-0.27}$ kpc ($1''$ corresponds to 2570 AU) based on trigonometric parallax measurement of 6.7 GHz methanol masers (Rygl et al. 2010). Although a distance of 1.8 kpc has been used for ON 1 by several authors (e.g., MacLeod et al. 1998; Kumar et al. 2004; Nagayama et al. 2008), we adopt the distance of 2.57 kpc in this paper. A massive star-forming clump (~ 300–$500\,M_\odot$ scaled to a distance of 2.57 kpc) $\sim$ 0.5 pc in size was detected from single-dish observations for the continuum at 0.35 mm and CS $J = 5$–4 line emissions in the region (Mueller et al. 2002; Shirley et al. 2003). Multiple YSOs are associated with this clump. The radio continuum emission at 8.4 GHz showed an UC H II region (Argon et al. 2000). Submillimeter array (SMA) observations detected five continuum emission sources at 345 GHz (defined as SMA 1–5) within a field of $\sim 5''$ (Su et al. 2009). Su et al. mentioned that the SMA 1 and 3 are hard to distinguish from the UC H II region observed by the 8.4 GHz radio continuum emission. Therefore, at least four YSOs exist within an area of only $5''$ (corresponding to ~ 13000 AU), those are the SMA 2, 4, 5, and the UC H II region. The water masers at 22.2 GHz in this area consist of two clusters (Downes et al. 1979), WMC 1 and 2 (defined in Nagayama et al. 2008). Nagayama et al. showed that the water masers in WMC 1 can be associated with a bipolar outflow on the basis of an east–west elongated structure and their internal proper motions. A corresponding large-scale outflow was observed by the CO $J = 2$–1 line (Kumar et al. 2004) and H_2 emission at 2.12 μm (Kumar et al. 2003). Some bipolar outflows exist; one of them, traced by $H^{13}CO^+$ $J = 1$–0 and SiO $J = 2$–1 line emission, shows outflows in the northeast–southwest direction at a position angle (PA) of $\sim 44°$ (Kumar et al. 2004). The ground-state hydroxyl masers at 1.665 and 1.667 GHz in this area are associated with the UC H II region (Nammahachak et al. 2006). A monitoring observation showed the expansion of hydroxyl masers at $\sim 5\,\mathrm{km\,s^{-1}}$, and the masers were thought to trace the expansion of the UC H II region (Fish & Reid 2007).

The 6.7 GHz methanol masers in ON 1 have two widely separated spectral features at velocities of $\sim 15\,\mathrm{km\,s^{-1}}$ ($V_{\rm lsr} \sim 0$, $15\,\mathrm{km\,s^{-1}}$: Menten 1991; Szymczak et al. 2000). The systemic velocity of this region based on the CS $J = 2$–1 line is $11.6 \pm 3.1\,\mathrm{km\,s^{-1}}$ (Bronfman et al. 1996). A different systemic velocity of $5.1 \pm 2.5\,\mathrm{km\,s^{-1}}$ has been observed using the H76α recombination line (Zheng et al. 1985). In either case, the systemic velocity is observed between the two methanol maser features. Since the kinematics of ON 1 were observed using various line emissions, including those of water and hydroxyl masers, this source is suitable for investigating the associated sites and evolutionary phases of the methanol masers.

Interferometric observations of the methanol masers in this region have been performed using the multi-element radio-linked interferometer network (MERLIN) by Green et al. (2007). They succeeded in mapping only red-shifted features ($V_{\rm lsr} = 14.46$ to $15.57\,\mathrm{km\,s^{-1}}$) because the bandwidth did not cover both features. VLBI observations for the ON 1 methanol masers, which covered both features, were conducted using the JVN (Sugiyama et al. 2008b) and the European VLBI network (EVN: Rygl et al. 2010). The image quality of this previous JVN observation did not allow for a detailed investigation of the structure because of poor uv-coverage and sensitivity.

3. Observations and Data Reduction

New JVN observations of ON 1 were conducted at three epochs: 2006 September 10, from 07:00 to 17:30 UT using four telescopes of the JVN; 2008 May 10 from 15:00 to 22:00 UT using five telescopes; and 2008 October 26, from 06:00 to 13:00 UT using six telescopes. The telescopes used in each observation are described in table 1 along with other observational parameters. The projected baselines ranged from 6 Mλ (Yamaguchi–Iriki) to 50 Mλ (Mizusawa–Ishigaki), corresponding to fringe spacings of 34.4 mas and 4.1 mas at 6.7 GHz, respectively.

A continuum source, J2003+3034 (1.°71 from ON 1), whose coordinates were determined with an accuracy of 0.55 mas in the second VLBA calibrator survey (VCS2) catalog (Fomalont et al. 2003), was used as a phase reference calibrator to obtain the absolute coordinates of the methanol masers. We alternately observed the ON 1 methanol masers and the continuum source with a cycle of 5 min (2 min on ON 1 and 1.8 min on the continuum source). ON 1 was sometimes observed continuously for more than 30 min to improve the uv-coverage in the first and second epochs. The total on-source times at each epoch were 3.4, 1.5, and 0.5 hr for ON 1 and 0.4, 0.7, and 0.3 hr for J2003+3034, respectively. Several radio continuum calibrators were also observed every hour for clock parameter correction (J2010+3322, J2023+3153, J2002+4725) and bandpass correction (3C 454.3, NRAO 530, DA 193).

In the first epoch, left-circular polarization was received at the Yamaguchi and Usuda stations, while linear polarization was received at the Mizusawa and Ishigaki stations. In the two epochs in 2008, left-circular polarization was received at the Yamaguchi, Usuda, Mizusawa, and Ishigaki stations, while at the Iriki and Ogasawara stations linear polarization was received. The data were recorded on magnetic tapes by using a VSOP terminal at a data rate of 128 Mbps with 2-bit quantization and two channels; they were correlated at the Mitaka FX correlator (Shibata et al. 1998). Of the recorded 32 MHz bandwidth, 2 MHz (6668–6670 MHz) was divided into 512 channels for obtaining high-velocity resolution in the maser reductions, yielding a velocity resolution of $0.18\,\mathrm{km\,s^{-1}}$ in 2006. The same velocity resolution was achieved in 2008, but the bandwidth and the number of channels were 4 MHz (6668–6672 MHz) and 1024, respectively. Single-dish observations were performed using the Yamaguchi 32 m telescope almost simultaneously with each VLBI observation. The spectral resolution of the single dish was four-times higher than that of the VLBI. The spectra obtained by the single-dish observations showed no variation during the three epochs.

Table 1. Parameters for ON 1 observations using the JVN.*

Epoch	Date	Telescopes†	$t_{\rm on}$	$1\,\sigma$	Synthesized beam		$N_{\rm spot}$
					$\theta_{\rm maj} \times \theta_{\rm min}$	PA	
	(y/m/d)		(hr)	(Jy beam^{-1})	(mas × mas)	(°)	
1	2006/09/10	Y, U, M, I	3.4	0.08	6.3 × 3.2	−59	36
2	2008/05/10	Y, M, R, O, I	1.5	0.20	4.6 × 3.1	−31	19
3	2008/10/26	Y, U, M, R, O, I	0.5	0.32	5.0 × 3.2	−54	23

* Column 1: epoch number; Column 2: observational year, month, and day; Column 3: telescopes used; Column 4: total on-source time; Column 5: rms of image noise in a line-free channel; Column 6–7: FWHMs of major and minor axes, and position angle of synthesized beam made in natural weight; Column 8: number of detected spots.
† Telescope code — Y: Yamaguchi, U: Usuda, M: VERA-Mizusawa, R: VERA-Iriki, O: VERA-Ogasawara, I: VERA-Ishigaki.

The VLBI data were reduced using the astronomical image processing system (AIPS: Greisen 2003). Correlator digitization errors were corrected using the task ACCOR. Delay and rate offsets were corrected by the task FRING by using the continuum calibrators. Bandpass calibration was performed by the task BPASS. Doppler corrections were performed by running the tasks SETJY and CVEL. Amplitude–gain calibration parameters were derived from the total power spectra of maser lines in W 75 North (W 75 N), a strong ($\sim$270–470 Jy), nearby ($\sim 11\overset{\circ}{.}5$) methanol maser source by using the template method in the task ACFIT. The primary amplitude unit was converted into janskys (Jy) on the basis of the single-dish spectrum observed using the Yamaguchi telescope by the same method. The conversion accuracy depends on the accuracy of the single-dish observations, $\sim 10\%$. Fringe fitting was conducted using a strong velocity channel at a local standard of rest (LSR) velocity of 0.00 km s^{-1} in the task FRING. Special amplitude calibrations, as described in Sugiyama et al. (2008b), were applied to different polarization correlations (circular/linear, linear/linear). The phase and amplitude solutions of self-calibration were calculated in the task CALIB by using the image of the velocity channel at 0.00 km s^{-1} formed by the task IMAGR. The solutions were applied to all other channels that contained maser emissions. We formed CLEAN images of each channel that included maser emissions by using the reference maser spot at an LSR velocity of 0.00 km s^{-1} in the task IMAGR with natural weighting. The full width at half maximum (FWHM) and the PA of the synthesized beams are given in table 1. The peak positions and peak intensities of maser spots were derived by fitting an elliptical Gaussian brightness distribution to each spot appearing in each image by using the task JMFIT. We identified maser spots on the basis of the signal-to-noise ratio (SNR) as well as the range of the velocity channels. All of the identified spots were more than five-times stronger than the rms noise level in the images for each spectral channel, and all appeared in multiple velocity channels.

4. Results

4.1. Spatial Distributions

We detected 36, 19, and 23 maser spots at epochs 1, 2, and 3, respectively, while the number of independent spots was 41. The peak intensities of the spots ranged from $\sim$0.3 to 30.9 Jy beam^{-1}, and the rms values of the image noise ($1\,\sigma$) in a line-free channel were 80, 200, and 320 mJy beam^{-1}, respectively. Given that 19 in 36 maser spots at the 1st epoch had peak intensities larger than 1 Jy beam^{-1} (corresponds to rms 5, $3\,\sigma$ of image noise at 2nd, 3rd epochs, respectively), the detection rates are almost the same above all epochs. The parameters of each maser spot are summarized in table 2. There are clearly flux variations for maser spots ID 5, 6, 15, 16, 18 according to the accuracies of the absolute flux, $\sim 10\%$. The relative positional accuracy of the methanol maser spots ranged over 0.01–0.80 mas, depending on the SNR and the spatial structure of the spot. The errors of fitting by an elliptical Gaussian were also included in the accuracy. The maser emissions were detected even with longer baselines, and the correlated flux accounted for over 90% of the single-dish flux.

The spatial distribution and the internal proper-motion vectors of the 6.7 GHz methanol maser spots in ON 1 are shown in figure 1 (for the proper motions, see subsection 4.2). The 36 spots detected at the first epoch within an area of $\sim$400 mas × 1100 mas ($\sim$1000 AU × 2800 AU) are plotted as dots with colors corresponding to $V_{\rm lsr}$. The origin of the map corresponds to the position of the reference spot with an LSR velocity of 0.00 km s^{-1}, whose absolute coordinates, obtained using a phase-referencing technique, are α(J2000.0) = $20^{\rm h}10^{\rm m}09\overset{\rm s}{.}0731$ and δ(J2000.0) = $+31^\circ31'35\overset{''}{.}934$ with an accuracy of 1 mas. The reference spot is also used as a reference for internal proper motion. We define three clusters of maser spots: the north (cluster I), southwest (II: $0\overset{''}{.}3$ west, $0\overset{''}{.}9$ south), and south (III: $0\overset{''}{.}1$ east, $1\overset{''}{.}0$ south) clusters. Cluster I had a radial-velocity range of $V_{\rm lsr} = -0.52$ to 1.59 km s^{-1}, whereas the other two clusters had ranges of $V_{\rm lsr} = 14.24$ to 15.12 and 14.24 to 14.77 km s^{-1} for clusters II and III, respectively. Cluster I was blue-shifted and clusters II and III were red-shifted relative to the systemic velocity. The blue-shifted maser spots were separated spatially as well as spectrally from the red-shifted ones.

The overall distribution of the ON 1 methanol masers coincided with that in the image obtained by Rygl et al. (2010). Clusters II and III correspond to C and D defined by Green et al. (2007). They also detected maser spots A and B in their MERLIN image, which were located at $0\overset{''}{.}4$ west, $0\overset{''}{.}8$ south and $0\overset{''}{.}2$ west, $0\overset{''}{.}9$ south, respectively, with respect to our reference maser spot, but we did not detect them in our VLBI image.

Table 2. Parameters of the 6.7 GHz methanol maser spots showing internal proper motion in ON 1.*

ID	LSR	Relative offset				Proper motion						Peak intensity		
	velocity	RA	σ_α	Dec	σ_δ	μ_α	$\sigma\mu_\alpha$	V_x	μ_δ	$\sigma\mu_\delta$	V_y	1st	2nd	3rd
	(km s^{-1})	(mas)				(mas yr^{-1})		(km s^{-1})	(mas yr^{-1})		(km s^{-1})	(Jy beam^{-1})		
(1)	(2)	(3)	(4)	(5)	(6)	(7)	(8)	(9)	(10)	(11)	(12)	(13)	(14)	(15)
						Cluster II								
1	14.77	−342.21	0.33	−897.43	0.24	—	—	—	—	—	—	0.42	—	—
2	14.59	−341.97	0.27	−897.83	0.18	—	—	—	—	—	—	1.67	—	—
3	14.94	−337.03	0.09	−879.56	0.08	0.31	0.11	3.76	−0.63	0.10	−7.68	3.57	4.69	2.88
4	14.77	−336.91	0.03	−880.29	0.03	−0.09	0.38	−1.05	−0.29	0.01	−3.53	12.37	14.69	14.20
5	14.59	−336.85	0.03	−880.68	0.02	−0.15	0.41	−1.84	−0.23	0.08	−2.76	15.77	17.20	26.31
6	14.41	−336.78	0.05	−880.93	0.03	−0.17	0.22	−2.13	−0.24	0.02	−2.98	7.79	8.23	18.51
7	14.24	−336.63	0.22	−881.16	0.16	−0.21	0.16	−2.55	−0.35	0.12	−4.30	1.37	1.59	5.14
8	15.12	−336.53	0.61	−879.99	0.41	—	—	—	—	—	—	0.42	—	—
						Cluster I								
9	−0.17	−3.52	0.34	−16.48	0.17	—	—	—	—	—	—	0.92	—	—
10	0.18	−3.48	0.36	−16.61	0.17	—	—	—	—	—	—	0.76	—	—
11	0.00	−3.29	0.30	−16.55	0.15	—	—	—	—	—	—	1.08	—	—
12	−0.70	−0.72	0.31	0.19	0.38	—	—	—	—	—	—	—	—	1.83
13	0.53	−0.61	0.26	0.60	0.18	—	—	—	—	—	—	0.74	2.08	1.77
14	0.36	−0.40	0.06	0.39	0.05	—	—	—	—	—	—	3.46	7.94	6.17
15	0.18	−0.21	0.02	0.18	0.02	—	—	—	—	—	—	9.19	18.83	17.85
16†	0.00	0.00	0.02	0.00	0.01	0.00	—	0.00	0.00	—	0.00	13.17	25.81	30.93
17	−0.52	0.07	0.19	−0.14	0.15	0.12	0.10	1.50	−0.13	0.08	−1.62	1.10	—	5.89
18	−0.17	0.22	0.02	−0.16	0.02	—	—	—	—	—	—	10.82	20.85	18.01
19	−0.35	0.39	0.04	−0.25	0.03	0.02	0.00	0.24	−0.04	0.02	−0.54	4.85	9.56	7.82
20	0.00	2.92	0.29	15.25	0.18	—	—	—	—	—	—	0.80	—	—
21	0.18	3.07	0.34	15.34	0.23	—	—	—	—	—	—	0.57	—	—
22	−0.17	3.39	0.31	15.05	0.16	—	—	—	—	—	—	0.72	—	—
23	1.06	5.88	0.63	40.63	0.46	0.55	0.33	6.77	0.64	0.25	7.81	0.42	—	0.94
24	0.88	6.54	0.43	40.73	0.32	—	—	—	—	—	—	—	—	0.66
25	1.06	7.79	0.45	−55.65	0.25	—	—	—	—	—	—	0.43	—	—
26	1.23	7.92	0.30	45.21	0.28	—	—	—	—	—	—	0.72	1.10	1.08
27	1.41	8.23	0.23	46.16	0.22	−0.15	0.14	−1.83	0.18	0.13	2.17	0.77	1.27	1.28
28	0.88	8.23	0.47	−55.85	0.27	—	—	—	—	—	—	0.39	—	—
29	1.06	8.51	0.59	43.02	0.43	—	—	—	—	—	—	0.49	—	—
30	1.59	8.57	0.43	46.19	0.41	—	—	—	—	—	—	0.38	—	—
						Cluster III								
31	14.41	63.44	0.29	−1015.34	0.23	—	—	—	—	—	—	—	1.55	7.81
32	14.24	63.76	0.33	−1015.13	0.32	—	—	—	—	—	—	—	1.13	4.60
33	14.59	64.04	0.17	−1014.96	0.12	—	—	—	—	—	—	—	3.35	5.32
34	14.59	67.34	0.29	−1014.07	0.13	—	—	—	—	—	—	2.35	3.19	—
35	14.41	67.56	0.27	−1013.99	0.12	0.45	0.17	5.52	−0.18	0.23	−2.15	2.62	3.21	6.21
36	14.24	69.02	0.35	−1013.80	0.22	−0.48	0.23	−5.85	−0.38	0.14	−4.63	1.01	1.09	4.03
37	14.77	73.07	0.65	−1011.05	0.28	—	—	—	—	—	—	1.20	—	—
38	14.41	75.09	0.16	−1009.99	0.12	−0.26	0.33	−3.19	−0.48	0.20	−5.90	2.18	—	3.93
39	14.59	76.10	0.57	−1009.41	0.26	—	—	—	—	—	—	1.07	—	—
40	14.24	78.06	0.41	−1008.45	0.19	—	—	—	—	—	—	0.98	—	—
41	14.41	79.29	0.41	−1008.61	0.30	—	—	—	—	—	—	0.62	—	—

* Column 1: spot identification number (in RA order); Column 2: LSR velocity; Columns 3–6: relative positional offsets with respect to the reference maser spot and uncertainties in the first epoch; Columns 7–12: internal proper motions, fitting errors, and tangential velocities for the right ascension and declination directions, respectively; Columns 13–15: peak intensities at each epoch.

† Reference spot for relative position and velocity. The absolute coordinates of the spot are given in the text.

4.2. Internal Proper Motions

Maser spots detected in different epochs were identified as being the same if their LSR velocities coincided within a velocity resolution of 0.18 km s^{-1} and their positions were within 2.7 mas at the first to third epochs (corresponding to a transversal velocity of ~ 15.5 km s^{-1} at 2.57 kpc, almost equivalent to the range of the radial velocity). On the basis of these criteria, 15 maser spots were identified at all three epochs; three spots were identified at the first and third epochs, and three spots were identified at the second and third epochs. The motions of 13 maser spots out of 21 identified spots were significantly larger than the relative positional uncertainties during the observation period. Our detection of the internal proper motions in ON 1 is one of the rare detections of the internal proper motions of the 6.7 GHz methanol masers (Sanna et al. 2008, 2010a, 2010b; Rygl et al. 2010). The internal proper-motion vectors are shown in figure 1, and the positional variations of each maser spot are shown in figure 2. The internal proper motions were measured by applying linear

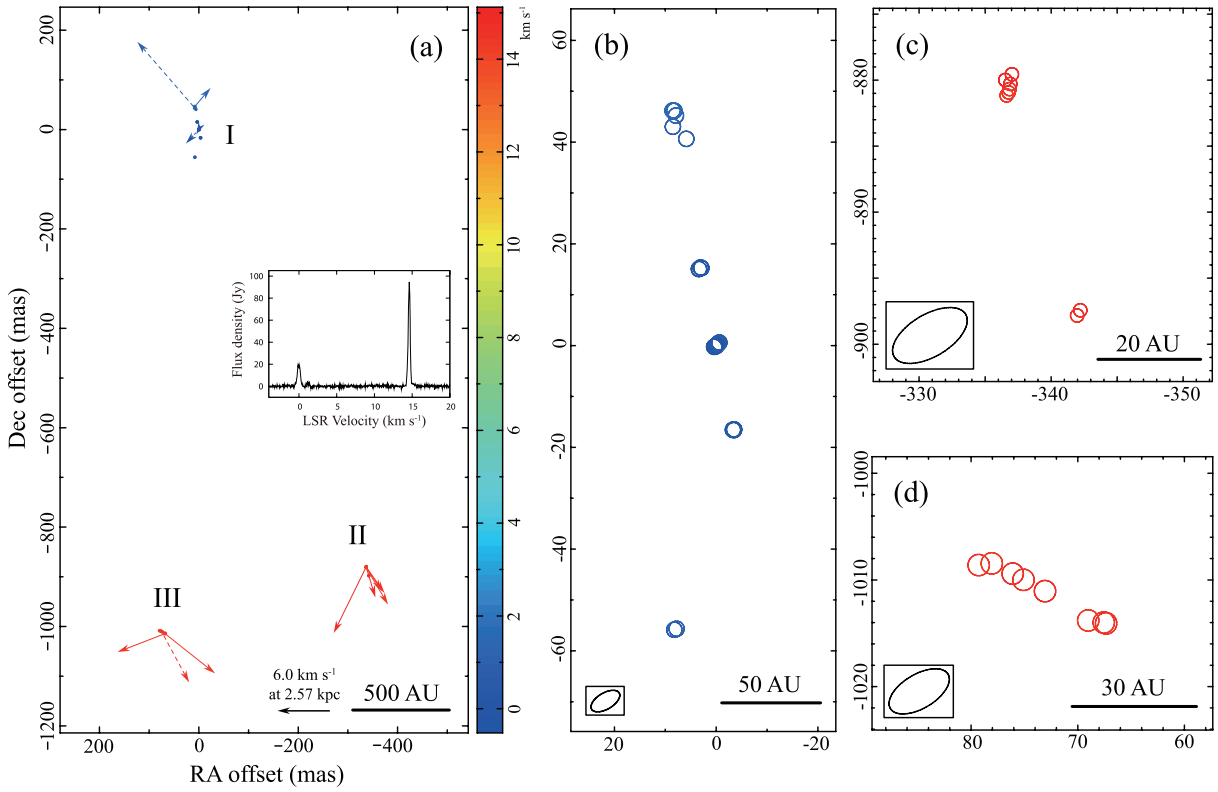

Fig. 1. (a) Spatial distribution and internal proper motions of the 6.7 GHz methanol maser spots (filled circle and arrow) of ON 1. The color indicates its radial velocity (see color index at the right). The labels I, II, and III indicate each maser cluster. The origin of this map corresponds to the absolute coordinates α(J2000.0) = $20^{\rm h}10^{\rm m}09^{\rm s}.0731$ and δ(J2000.0) = $+31^\circ31'35''.934$. Arrows show proper motion of spots, and their lengths are proportional to the tangential velocities. The spatial and velocity scales are shown in the lower corner. The solid arrows show the motions detected at all three epochs, while the dashed arrows show ones detected in only two (first and third) epochs. The spectrum of the ON 1 methanol maser by single-dish observation using Yamaguchi 32 m telescope is also shown in the middle frame. The velocity resolution is 0.044 km s^{-1}, which is four-times smaller than that of the VLBI observations (0.18 km s^{-1}). (b)–(d) Blow-up figures of clusters I, II, and III, respectively. Open circles show the methanol maser spots in a fixed scale. Each ellipse at the bottom-left corner in each figure corresponds to a synthesized beam.

motion to the positional offsets on the timeline. The results of the internal proper-motion measurements are also given in table 2.

As can be seen in figure 1, the internal proper motions reflected outward motions in roughly the north–south direction. The declination components of the proper motions, μ_δ, ranged from -0.63 to $+0.64$ mas yr^{-1}, which corresponds to tangential velocities, V_y, ranging from -7.7 to $+7.8$ km s^{-1}. The averaged north–south velocities were 0.8 ± 1.6 km s^{-1} for cluster I ($V_{\rm I}$) and -4.2 ± 0.7 km s^{-1} for clusters II and III ($V_{\rm II,III}$) (north is positive). The difference between these velocities, $V_{\rm I} - V_{\rm II,III}$, is 5.0 km s^{-1}.

The outward motions in roughly the north–south direction clearly suggest that a rotating disk is unlikely to be the site associated with the 6.7 GHz methanol masers in ON 1. A simple explanation for the outward motion is that these masers are associated with an expanding shell or a bipolar outflow if we assume that the motion can be explain by mono-phenomenon. The north–south velocity $V_{\rm I} - V_{\rm II,III}$ of 5.0 km s^{-1} is comparable to the typical motion velocities of OH masers associated with an expanding shell (Bloemhof et al. 1992; Fish & Reid 2007). On the other hand, the direction of the outward motion is similar to that of the $H^{13}CO^+$ and SiO outflows (Kumar et al. 2004), which was roughly distributed in the north–south direction.

5. Discussion

5.1. *Spatial Relationship*

In figure 3, we have superposed the 6.7 GHz methanol masers in ON 1 (open squares) on the 22.2 GHz water masers (open circles, Nagayama et al. 2008), hydroxyl masers at 1.665 and 1.667 GHz (crosses, Fish & Reid 2007), and continuum emission at 8.4 GHz (white contours, Argon et al. 2000) and at 345 GHz (stars, Su et al. 2009). The arrows indicate the directions of the northeast–southwest bipolar outflow traced by $H^{13}CO^+$ and SiO lines (Kumar et al. 2004), and the dashed line represents the axis of the east–west bipolar outflow observed in the CO $J = 2$–1 line, and discussed by Nagayama et al. (2008). The absolute positional accuracy of the methanol masers was 1 mas, and those of the water and hydroxyl masers were $\sim$80 mas and 200 mas, respectively. Those of the 8.4 GHz and 345 GHz continuum emissions were $\sim0''.3$ and $\sim0''.1$, respectively.

Note that each cluster of the methanol maser spots coincided spatially with a cluster of hydroxyl masers (defined in figure 1

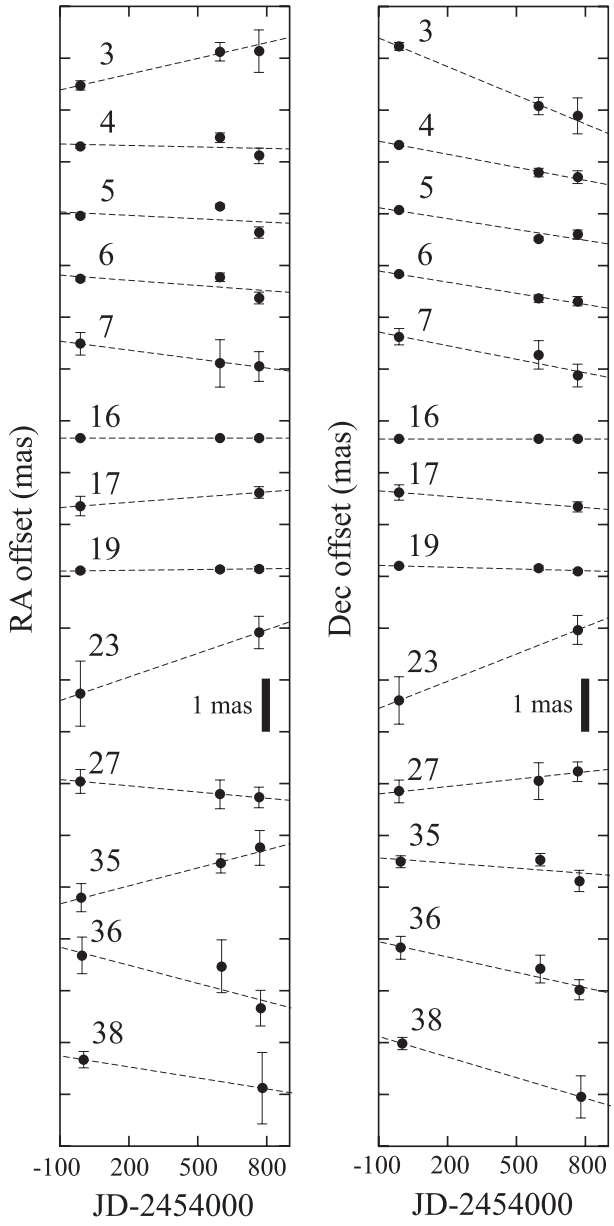

Fig. 2. Positional variation in each direction (RA and Dec) of the methanol maser spots of ON 1 during the observation period. Numbers are the spot ID in table 2. The dash lines indicate a linear fit.

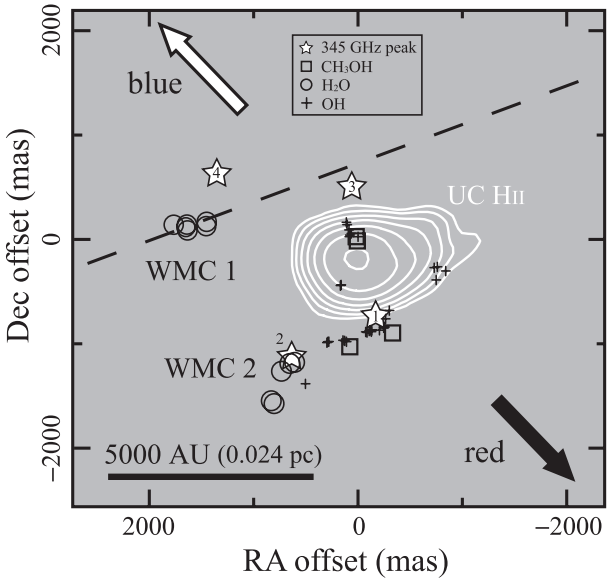

Fig. 3. Observed methanol maser distribution (open squares) superposed on the 8.4 GHz radio continuum map (white contours) of the UC H II region (Argon et al. 2000). The star symbols correspond to the positions of the brightness peak of the dust emissions at 345 GHz and their number denote the SMA 1–4 (Su et al. 2009), while the SMA 5 locates out of this figure. The average sizes of the dust emissions are $\sim$1 arcsec^2. The water maser (Nagayama et al. 2008) and the hydroxyl maser distributions (Fish & Reid 2007) are shown by open circles and crosses, respectively. The WMC 1 and 2 were defined in Nagayama et al. (2008). The arrows represent the directions of the NE–SW bipolar outflows traced by the $H^{13}CO^+$ $J = 1$–0 and SiO $J = 2$–1 lines (Kumar et al. 2004). The colors of black and white correpond to the red- and blue-shifted sides with respect to the systemic velocity. The dashed line indicates the axis of the E–W bipolar outflow observed in the CO $J = 2$–1 line (Kumar et al. 2004).

of Fish & Reid 2007): cluster I to the N cluster, cluster II to the SW cluster, and cluster III to the SE cluster. These two types of masers also have similar LSR velocity ranges: -0.52 to 15.12 and 2.48 to 16.73 km s^{-1} for methanol and hydroxyl masers, respectively. The hydroxyl masers were thought to be associated with the expanding UC H II region because their internal proper motions showed an expansion with respect to the center of the peak of the 8.4 GHz continuum emission. A coincidence between the methanol and hydroxyl masers was suggested by a maser-excitation model (Cragg et al. 2002). According to the model, a physical condition that produces simultaneous population inversions in both the 6.7 GHz methanol and 1.6 GHz hydroxyl transitions by infrared radiation is achieved.

On the other hand, the water masers of WMC 1 were clearly separated from the methanol and hydroxyl masers, with a positional offset of $\sim 1\farcs5$, i.e., $\sim$4000 AU at 2.57 kpc. The LSR velocities of the water masers also differed from those of the methanol and hydroxyl masers, showing far higher velocities and a wider range of $V_{\rm lsr}$(~ -60 to 60 km s^{-1}). Nagayama et al. (2008) suggested that the two clusters of water masers (WMC 1 and 2) would be associated with YSOs at around the dust emission peaks at 345 GHz (SMA 4 and 2). Theoretical models of water-maser excitation (Elitzur et al. 1992) predicted that water masers were produced by collisional pumping within shocked layers.

The distinctions between the methanol and hydroxyl masers and the water masers in ON 1 in terms of their spatial distributions and radial/tangential velocities can also be understood in terms of the types of associated sources. These results suggest that methanol and hydroxyl masers are excited by different sources at separate sites and by different pumping mechanisms from those of the water masers.

The three clusters of the 6.7 GHz methanol maser in ON 1 are spatially isolated with a scale of $\sim$2800 AU at maximum. Are the clusters physically associated with and excited by a common source? We think that the physical association is true because of two reasons, as follows: firstly, three

radio continuum sources, which consist of centimeter (UC H II region) and two submillimeter (dust: SMA 1 and 3) emissions, are detected around the location of the methanol maser clusters. As mentioned in section 2, Su et al. (2009) eventually concluded that the SMA 1 and 3 were just dust emissions associated with the UC H II region, that is that the SMA 1 and 3 do not include YSOs. Thus, there is only one massive star around the location of the clusters. Secondary, some methanol maser emissions have shown periodic variation of flux density with synchronization above all spectral features (e.g., Goedhart et al. 2003, 2009). Those maser spots were distributed in a scale of $\sim$6000 AU at maximum, which corresponds to a size approximately two times larger than that in the case of ON 1. The synchronized time variation of the masers are explained as being because all of the maser spots are pumped by infrared radiation from the dust that is heated by a common exciting source with a rapid variability (Sugiyama et al. 2008a). Thus, the methanol maser clusters in ON 1 isolated at $\sim$2800 AU can be pumped with one exciting source. We therefore expect that all three clusters of the 6.7 GHz methanol masers can be excited by a common massive star that forms the UC H II region.

5.2. *Sites Associated with the Methanol Masers*

Rotational disks and shock regions formed by the outflow have been considered to be the main candidates for sites associated with methanol masers at 6.7 GHz in massive star-forming regions. We discuss the following three possibilities for sites associated with methanol masers in ON 1: (i) a disk, (ii) an expanding shell, and (iii) a bipolar outflow.

First, are the methanol masers in ON 1 associated with a disk? As mentioned in subsection 4.2, the outward motions in the north–south direction detected in the internal proper motions of the methanol masers clearly eliminates the disk model. The separation of the red- and blue-shifted spectral features of $\sim 15\,\mathrm{km\,s^{-1}}$ of radial velocities is so wide that the central mass estimated by simple Keplerian rotation, $\sim 100\,M_\odot$ (using half the velocity and the spatial extent of the distribution of methanol masers to define the diameter of the disk), is not consistent with the typical mass of a star located in an UC H II region, $\sim 15\,M_\odot$, which is inferred from its spectral type of B0 (MacLeod et al. 1998). These properties do not agree with the rotating-disk model, and thus this model is unlikely.

Second, are the methanol masers in ON 1 associated with the expanding UC H II region as well as with the hydroxyl masers? As described in subsection 5.1, the methanol masers in ON 1 coincide spatially with the hydroxyl masers. The radial-velocity ranges and the internal proper motions of the methanol masers were also quite similar to those of the hydroxyl masers, at least where the two types coincided spatially. Rygl et al. (2010) also detected the internal proper motions of the 6.7 GHz methanol masers in ON 1 in the north–south direction with the EVN, and suggested that the methanol masers would be located in the molecular gas surrounding the expanding UC H II region.

There are radial-velocity differences between the 6.7 GHz methanol and the 1.665 GHz hydroxyl masers in cluster I: methanol $V_{\rm lsr}$ from -0.7 to $1.6\,\mathrm{km\,s^{-1}}$, while hydroxyl $V_{\rm lsr}$ from 2.5 to $6.1\,\mathrm{km\,s^{-1}}$. In the 1.665 GHz hydroxyl masers, almost all spots correspond to left-circular polarization (LCP) emissions (9 in the 12 spots: Fish & Reid 2007). Thus, the difference in the radial velocities could be due to the Zeeman-splitting effects in the area around cluster I. Fish (2007) measured the strengthes of the magnetic fields around the cluster I by the 6.035 GHz hydroxyl maser, which range from -8.7 to -12.1 mG. If we assume a magnetic field of averaged -10 mG around cluster I, similar to that seen in the case of the 6.035 GHz hydroxyl maser by Fish (2007), LCP and RCP of the 1.665 GHz maser features would be separated by $5.9\,\mathrm{km\,s^{-1}}$ according to the Zeeman-splitting coefficient, $0.59\,\mathrm{km\,s^{-1}mG^{-1}}$ at 1.665 GHz (Davies 1974). For the 1.665 GHz hydroxyl maser LCP features at $V_{\rm lsr}$ from 3.1 to $6.1\,\mathrm{km\,s^{-1}}$ in the north cluster, these might have pairs of RCP features at $V_{\rm lsr}$ from -2.8 to $0.2\,\mathrm{km\,s^{-1}}$. On the other hand, the 6.7 GHz methanol maser indicates a Zeeman-splitting coefficient of $4.9\times10^{-5}\,\mathrm{km\,s^{-1}mG^{-1}}$ (Vlemmings et al. 2006; Vlemmings 2008), which leads to a separation of $4.9\times10^{-4}\,\mathrm{km\,s^{-1}}$ between the LCP and RCP features: essentially no change in the radial velocity. Hence, the suspected radial velocities of the 1.665 GHz hydroxyl RCP features would correspond to those of the 6.7 GHz methanol masers, and the LCP spots of the 1.665 GHz hydroxyl maser would have radial velocities higher than those of the 6.7 GHz methanol maser. Those RCP components would have flux densities weaker than the image sensitivities in Fish et al. (2005) and Fish and Reid (2007).

Finally, we present another possibility for the associated sites: the methanol masers in ON 1 might be associated with the $H^{13}CO^+$ and SiO outflows. As mentioned in subsection 4.2, the internal proper motions of the methanol masers showed a flow direction similar to that of the $H^{13}CO^+$ and SiO outflows: the motions were roughly in the north–south direction, away from the reference maser spot. The radial velocities of the methanol masers were shifted with respect to the systemic velocity in the same direction as the $H^{13}CO^+$ and SiO outflows; the northeast and southwest components of both types of masers and of the outflows were blue- and red-shifted, respectively. The difference in the mean velocities of the north and south components of the proper motion, $V_{\rm I} - V_{\rm II,III}$, was $5.0\,\mathrm{km\,s^{-1}}$, which was roughly equal to the velocity of the $H^{13}CO^+$ outflow, $4.5\,\mathrm{km\,s^{-1}}$. These results suggest that the 6.7 GHz methanol masers in ON 1 could have the same kinematics as the $H^{13}CO^+$ and SiO outflows. To confirm whether the maser spots are moving toward the $H^{13}CO^+$ and SiO outflows, the absolute proper motions of the methanol masers in ON 1 must be measured.

We note that the spatial extent of the maser spot distribution was $\sim$30-times smaller than that of the observed $H^{13}CO^+$ outflow, and the velocity gradients of the methanol masers and the $H^{13}CO^+$ line differ. The velocity gradient for the methanol masers was $7.0\times10^{-3}\,\mathrm{km\,s^{-1}AU^{-1}}$, more than an order of magnitude steeper than that for the $H^{13}CO^+$ line, $2.1\times10^{-4}\,\mathrm{km\,s^{-1}AU^{-1}}$. This difference might arise from the difference in the spatial resolutions ($\sim$1000 times) of the observations.

5.3. *Evolutionary Phase*

It has been discussed whether methanol or water masers appear at an earlier evolutionary phase of massive star

formation. We compare the types of continuum sources associated with the water masers in WMC 1 and with the methanol masers we observed. The water masers of WMC 2, which is located at SMA 2, are excluded from this discussion, because they may be associated with an intermediate-mass star-forming core (Su et al. 2009).

As mentioned in subsection 5.1, the water masers of WMC 1 are associated with a peak of dust emission (submillimeter continuum source), whereas the methanol masers were associated with an UC H II region (centimeter continuum source) in ON 1. The mass of SMA 4, which could excite the water masers in WMC 1, is 6.4 $M_\odot$ (Su et al. 2009). They concluded that SMA 4 was the brightest and the most massive source among SMA 1–5; it was thought to mark a star-forming site in a very early evolutionary phase, because it was not associated with any of the signatures of star formation. This source, therefore, is thought to form a massive star by accreting gases from its associated large-scale clump (Mueller et al. 2002; Shirley et al. 2003). On the other hand, the mass of the star in the UC H II region is $\sim 15\,M_\odot$, which was inferred from its spectral type of approximately B0 (MacLeod et al. 1998). If the dust emission source SMA 4 forms a massive star, as suggested above, the dust emission source is obviously in a younger phase than the UC H II region, which is produced by a well-evolved star embedded in the region. These properties of the associated sites suggest that the water maser appeared earlier than the methanol maser in the evolutionary phase of ON 1.

This result is also supported by a comparison of the dynamical ages associated with each type of maser, if we assume that the methanol masers are associated with the $H^{13}CO^+$ outflow. Nagayama et al. (2008) suggested that the water masers of WMC 1 were associated with the bipolar outflow in the east–west direction observed by the CO $J = 2$–1 line and H_2 emission at 2.12 μm elongated by ~ 0.1 pc. They derived the dynamical age of the CO outflow as $\sim 10^4$ yr by using the size, ejection velocities, and the inclination angle of the outflow. The dynamical age of the $H^{13}CO^+$ outflow (with a size of ~ 0.38 pc) is estimated to be 8×10^4 yr, assuming a velocity of 4.5 km s^{-1}.

This result is a case study for the massive star-forming region ON 1. For investigating a general relation of evolutionary phases between the methanol and water masers, we need to increase the observational samples, such like the ON 1 case study in the near future.

6. Conclusion

We have presented the distribution and internal proper motions of the 6.7 GHz methanol masers in ON 1 measured with the JVN at three epochs spanning 778 days. The methanol maser spots were clustered and distributed within an area of ~ 1000 AU $\times$ 2800 AU. The radial velocities of northern and southern clusters were blue- and red-shifted, respectively. The distribution coincided with that of the hydroxyl masers, which surround an UC H II region. The methanol masers showed outward motions in roughly the north–south direction. The relative outward velocity is ~ 5 km s^{-1}, and the motion is also similar to that of the hydroxyl masers. These two masers, therefore, probably trace the same kinematics, that is, the expanding UC H II region. On the other hand, the distribution and velocity of the methanol masers are also similar to those of the $H^{13}CO^+$ $J = 1$–0 and SiO $J = 2$–1 outflows. The methanol masers in ON 1 might be associated with these outflows.

In comparing the associated sites, we found that the water masers appear in an earlier phase of YSO evolution than the methanol masers in ON 1: the water masers were associated with dust emission, whereas the methanol masers were associated with the UC H II region, which is in a later evolutionary phase than the dust core. This conclusion is supported by the dynamical ages of the CO $J = 2$–1 and $H^{13}CO^+$ outflows observed in ON 1.

One of the authors (Koichiro Sugiyama) is a Research Fellow DC2 of the Japan Society for the Promotion of Science (JSPS), and this study was supported by a Grant-in-Aid for Scientific Research (No. 21-10375) from the JSPS. The authors thank the JVN team for assistance and support during the observations. The authors also thank an anonymous referee for many useful suggestions and comments, which improved this paper. The JVN project is led by the National Astronomical Observatory of Japan, which is a branch of the National Institutes of Natural Sciences, Hokkaido University, The University of Tsukuba, Ibaraki University, Gifu University, Osaka Prefecture University, Yamaguchi University, and Kagoshima University, in cooperation with the Geographical Survey Institute, the Japan Aerospace Exploration Agency, and the National Institute of Information and Communications Technology.

References

Argon, A. L., Reid, M. J., & Menten, K. M. 2000, ApJS, 129, 159
Bartkiewicz, A., Szymczak, M., & van Langevelde, H. J. 2005, A&A, 442, L61
Bartkiewicz, A., Szymczak, M., van Langevelde, H. J., Richards, A. M. S., & Pihlström, Y. M. 2009, A&A, 502, 155
Beuther, H., Walsh, A., Schilke, P., Sridharan, T. K., Menten, K. M., & Wyrowski, F. 2002, A&A, 390, 289
Bloemhof, E. E., Reid, M. J., & Moran, J. M. 1992, ApJ, 397, 500
Bronfman, L., Nyman, L.-A., & May, J. 1996, A&AS, 115, 81
Cragg, D. M., Sobolev, A. M., & Godfrey, P. D. 2002, MNRAS, 331, 521
Davies, R. D. 1974, in IAU Symp. 60, Galactic Radio Astronomy, ed. F. J. Kerr & S. C. Simonson (Dordrecht: Reidel), 275
De Buizer, J. M. 2003, MNRAS, 341, 277
Dodson, R., Ojha, R., & Ellingsen, S. P. 2004, MNRAS, 351, 779
Downes, D., Genzel, R., Moran, J. M., Johnston, K. J., Matveyenko, L. I., Kogan, L. R., Kostenko, V. I., & Ronnäng, B. 1979, A&A, 79, 233
Elitzur, M., Hollenbach, D. J., & McKee, C. F. 1992, ApJ, 394, 221
Ellingsen, S. P., Voronkov, M. A., Cragg, D. M., Sobolev, A. M., Breen, S. L., & Godfrey, P. D. 2007, in IAU Symp. 242, Astrophysical Masers and their Environments (Cambridge: Cambridge University Press), 213

Fish, V. L. 2007, ApJ, 669, L81
Fish, V. L., & Reid, M. J. 2007, ApJ, 670, 1159
Fish, V. L., Reid, M. J., Argon, A. L., & Zheng, X.-W. 2005, ApJS, 160, 220
Fomalont, E. B., Petrov, L., MacMillan, D. S., Gordon, D., & Ma, C. 2003, AJ, 126, 2562
Fujisawa, K. 2008, in Proc. 9th European VLBI Network Symp., POS (IX EVN Symposium) (Trieste: SISSA), 75
Goddi, C., Moscadelli, L., Sanna, A., Cesaroni, R., & Minier, V. 2007, A&A, 461, 1027
Goedhart, S., Gaylard, M. J., & van der Walt, D. J. 2003, MNRAS, 339, L33
Goedhart, S., Langa, M. C., Gaylard, M. J., & van der Walt, D. J. 2009, MNRAS, 398, 995
Green, J. A., Richards, A. M. S., Vlemmings, W. H. T., Diamond, P., & Cohen, R. J. 2007, MNRAS, 382, 770
Greisen, E. W. 2003, in Information Handling in Astronomy — Historical Vistas, ed. A. Heck (Dordrecht: Kluwer Academic Publishers), 109
Kumar, M. S. N., Davis, C. J., & Bachiller, R. 2003, Ap&SS, 287, 191
Kumar, M. S. N., Tafalla, M., & Bachiller, R. 2004, A&A, 426, 195
MacLeod, G. C., Scalise, E., Jr., Saedt, S., Galt, J. A., & Gaylard, M. J. 1998, AJ, 116, 1897
Menten, K. M. 1991, ApJ, 380, L75
Minier, V., Booth, R. S., & Conway, J. E. 2000, A&A, 362, 1093
Minier, V., Ellingsen, S. P., Norris, R. P., & Booth, R. S. 2003, A&A, 403, 1095
Moscadelli, L., Goddi, C., Cesaroni, R., Beltrán, M. T., & Furuya, R. S. 2007, A&A, 472, 867
Mueller, K. E., Shirley, Y. L., Evans, N. J., II, & Jacobson, H. R. 2002, ApJS, 143, 469
Nagayama, T., Nakagawa, A., Imai, H., Omodaka, T., & Sofue, Y. 2008, PASJ, 60, 183
Nammahachak, S., Asanok, K., Hutawarakorn Kramer, B., Cohen, R. J., Muanwong, O., & Gasiprong, N. 2006, MNRAS, 371, 619
Phillips, C. J., Norris, R. P., Ellingsen, S. P., & McCulloch, P. M. 1998, MNRAS, 300, 1131
Reid, M. J. 2007, in IAU Symp. 242, Astrophysical Masers and their Environments (Cambridge: Cambridge University Press), 522
Rygl, K. L. J., Brunthaler, A., Reid, M. J., Menten, K. M., van Langevelde, H. J., & Xu, Y. 2010, A&A, 511, A2
Sanna, A., Moscadelli, L., Cesaroni, R., Tarchi, A., & Furuya, R. S. 2008, in Proc. 9th European VLBI Network Symp., POS (IX EVN Symposium) (Trieste: SISSA), 91
Sanna, A., Moscadelli, L., Cesaroni, R., Tarchi, A., Furuya, R. S., & Goddi, C. 2010a, A&A, 517, A71
Sanna, A., Moscadelli, L., Cesaroni, R., Tarchi, A., Furuya, R. S., & Goddi, C. 2010b, A&A, 517, A78
Shibata, K. M., Kameno, S., Inoue, M., & Kobayashi, H. 1998, ASP Conf. Ser., 144, 413
Shirley, Y. L., Evans, N. J., II, Young, K. E., Knez, C., & Jaffe, D. T. 2003, ApJS, 149, 375
Su, Y.-N., Liu, S.-Y., & Lim, J. 2009, ApJ, 698, 1981
Sugiyama, K., Fujisawa, K., Doi, A., Honma, M., Isono, Y., Kobayashi, H., Mochizuki, N., & Murata, Y. 2008a, PASJ, 60, 1001
Sugiyama, K., Fujisawa, K., Doi, A., Honma, M., Kobayashi, H., Bushimata, T., Mochizuki, N., & Murata, Y. 2008b, PASJ, 60, 23
Surcis, G., Vlemmings, W. H. T., Dodson, R., & van Langevelde, H. J. 2009, A&A, 506, 757
Szymczak, M., Hrynek, G., & Kus, A. J. 2000, A&AS, 143, 269
Torstensson, K. J. E., van Langevelde, H. J., Vlemmings, W. H. T., & Bourke, S. 2010, arXiv:1010.4191
Torstensson, K., van Langevelde, H. J., Vlemmings, W., & van der Tak, F. 2008, in Proc. 9th European VLBI Network Symp., POS (IX EVN Symposium) (Trieste: SISSA), 39
Vlemmings, W. H. T. 2008, A&A, 484, 773
Vlemmings, W. H. T., Harvey-Smith, L., & Cohen, R. J. 2006, MNRAS, 371, L26
Vlemmings, W. H. T., Surcis, G., Torstensson, K. J. E., & van Langevelde, H. J. 2010, MNRAS, 404, 134
Walsh, A. J., Burton, M. G., Hyland, A. R., & Robinson, G. 1998, MNRAS, 301, 640
Xu, Y., Li, J. J., Hachisuka, K., Pandian, J. D., Menten, K. M., & Henkel, C. 2008, A&A, 485, 729
Zheng, X. W., Ho, P. T. P., Reid, M. J., & Schneps, M. H. 1985, ApJ, 293, 522